Electrical conductivity, thermoelectrical properties, and EPR spectroscopy of copper chromite ceramic samples doped with magnesium

V. A. Kulbachinskii, V. G. Kytin, D. Yu. Kondratieva, E. A. Konstantinova, A. V. Pavlikov, A. N. Grigoriev, A. S. Mankevich, and I. E. Korsakov

View Online   Export Citation   CrossMark

ARTICLES YOU MAY BE INTERESTED IN

Electrical conductivity, thermoelectrical properties, and EPR spectroscopy of copper chromite ceramic samples doped with magnesium

V. A. Kulbachinskii,[1,2,3,4,a)] V. G. Kytin,[1,5] D. Yu. Kondratieva,[1] E. A. Konstantinova,[1] A. V. Pavlikov,[1] A. N. Grigoriev,[1] A. S. Mankevich,[1] and I. E. Korsakov[1]

AFFILIATIONS

[1] Lomonosov Moscow State University, GSP-1, Leninskie Gory, Moscow, 119991, Russia
[2] Moscow Institute of Physics and Technology (MIPT), Dolgoprudny, Moscow region, 141700, Russia
[3] National Research Nuclear University — Moscow Engineering Physics Institute (NRNU-MEPhI), Moscow, 115409, Russia
[4] National Research Center "Kurchatov Institute", Moscow, 123182, Russia
[5] VNIIFTRI, Mendeleevo, Moscow region, 141570, Russia

[a)] Email: kulb@mig.phys.msu.ru

ABSTRACT

The results of a study of copper chromite ceramic samples doped with magnesium are presented. The samples were synthesized according to the solid-phase method using a special procedure for preparing the initial mixture, which ensures a uniform distribution of magnesium with its content from 0.2 to 6%. The substitution of chromium for magnesium in the crystal lattice is confirmed by Raman scattering of light and EPR spectra. As the magnesium content increases from 0 to 6 at.%, the resistivity of the synthesized samples decreases by more than 3 orders of magnitude at room temperature. High thermopower values were obtained, and it was shown that the main charge carriers are holes, and the predominant mechanism of hole transport in doped samples is hopping transfer over localized states, whose density decreases with an increase in energy near the Fermi energy. It is shown that the localization radius increases with an increase in magnesium content.

INTRODUCTION

Chromite copper belongs to the class of delafossites[1]; this material is conductive and transparent to visible light. In addition, this material has hole conductivity,[1–3] and the number of known transparent p-type semiconductors is strongly limited. This makes copper chromite promising for applications in optoelectronics. Recently it was discovered that copper chromite exhibits large values of the Seebeck coefficient that are weakly dependent on temperature, which also makes it promising for thermoelectric applications,[1,4] The main problem associated with the use of copper chromite in electronics is its low electrical conductivity.[1–5] It was shown that, in order to increase the electrical conductivity, copper chromite can be doped with elements of group II of the periodic table.[3–8]

The dopant behavior and charge transfer mechanisms in the doped copper chromite remain largely unexplored and unexplained. This is related to the complexity of the electronic structure of copper chromite,[1,9,10] the rather high polarizability of the crystal lattice,[11] and the presence of a quasi-two-dimensional lattice of magnetic chromium ions.[12–14] In addition, there are significant experimental difficulties in obtaining copper compounds with a valence of I with a uniform distribution of the dopant. In the context of the above, the study of doped copper chromite is relevant both from a scientific and practical points of view.

The purpose of this work is the synthesis of homogeneous copper chromite samples doped with magnesium, the study of electrical conductivity, thermoelectric properties,

and electron paramagnetic resonance (EPR) for copper chromite with different magnesium content.

1. SYNTHESIS AND CHARACTERIZATION OF SAMPLES

Samples of the $CuCr_{1-x}Mg_xO_2$ ceramics, where $x = 0$, 0.002, 0.008, 0.015, 0.03, and 0.06, were synthesized and studied in the present work. Synthesis was carried out according to the nitrate method. Synthesis of doped samples for uniform distribution of impurities in the samples (up to the 0.2% concentration of magnesium) began with obtaining a homogeneous mixture of chromium, copper, and magnesium oxides *via* the liquid phase. The source oxides were obtained by thermolysis of Cr, Mg, and Cu in the NH_4NO_3 melt according to the following reactions:

$$Cu(NO_3)_2 \cdot 3H_2O \rightarrow CuO + 2NO_2 \uparrow + 1/2O_2 \uparrow + 3H_2O \uparrow, \quad (1)$$

$$Mg(NO_3)_2 \cdot 6H_2O \rightarrow MgO + 2NO_2 \uparrow + 1/2O_2 \uparrow + 6H_2O \uparrow, \quad (2)$$

$$2Cr(NO_3)_3 \cdot 9H_2O \rightarrow Cr_2O_3 + 6NO_2 \uparrow + 3/2O_2 \uparrow + 9H_2O \uparrow, \quad (3)$$

$$NH_4NO_3 \rightarrow NH_3 + HNO_3. \quad (4)$$
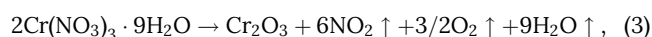
The calculated amounts of Cr, Mg, and Cu nitrates were mixed in a glass in a dry crystalline form. An equal weight of NH_4NO_3 was added to the resulting mixture of salts. The mixture was heated on a sand bath until melting (dissolving the salts in their own water of crystallization at a temperature of about 100°C), and the decomposition of mixtures of nitrates was carried out in the NH_4NO_3 melt. As decomposition occurs in a fraction of a second – in fact, in an explosive manner – decomposition was carried out in small 5 g portions of the mixture of salts in 10 steps. Portions of 5 g of crystalline NH_4NO_3 were added to each portion (5 g) of the dry mixture of metal nitrates, stirred and placed in a 0.6 l beaker, and then placed in a sand bath. The powder melted in its own water of crystallization at 100°C. A complete disappearance of the precipitate and the formation of a dark-green regular solution were achieved by stirring. The solution was left in a sand bath for 5 minutes; this was followed by its boiling and a sharp powerful decomposition, accompanied by the release of smoke, brown vapor, and partial dispersion of the thermolysis product powder. A black-brown powder of decomposition products of nitrates was obtained in the glass after cooling and collected. The thermolysis procedure was carried out with new portions of the mixture of salts. The thermolysis product was annealed in a furnace at 500°C for 30 min for the final decomposition of nitrates; then, it was milled, pressed into tablets with a diameter of 25 mm, and sintered in an argon stream at 1000–1100°C, at which the following reaction proceeded

$$2CuO + (1-x)Cr_2O_3 + (2x)MgO \rightarrow 2CuCr_{1-x}Mg_xO_2 + 1/2O_2 \uparrow. \quad (5)$$
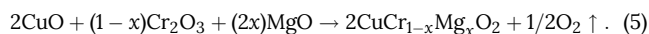
After sintering, the samples were cooled with the furnace in a stream of high-purity argon to prevent possible oxidation of copper with oxygen. This synthesis procedure ensured the uniformity of the distribution of magnesium in the sample in the case of its low content.

The structure and composition of the synthesized samples were studied by X-ray phase analysis. According to the obtained diffraction patterns, examples of which are shown in Fig. 1, samples containing magnesium up to $x = 0.03$ inclusive, were phase-pure delafossite (silicon was added as a reference).

The $MgCr_2O_4$ spinel impurity phase appears in the sample with magnesium content $x = 0.06$. Consequently, the boundary of the homogeneity region of the $CuCr_{1-x}Mg_xO_2$ solid solution lies between 3 and 6 at.% of magnesium. The lines of silicon added to determine the lattice parameters are also indicated in Fig. 1, except for the lines of delafossite and spinel.

Raman spectra were measured at room temperature for an additional study of the structure of samples; excitation was performed using a He–Ne laser with a wavelength of 632.7 nm. In order to avoid overheating of the sample by laser radiation, the laser radiation power was selected in such a way that, when it is increased by 3 times, the shift of the maxima of the main lines did not exceed 0.2 cm⁻¹. The measured Raman spectra are presented in Fig. 2. Only two intense lines from the phonon modes A_{1g} and E_g and diffuse features from the phonon modes $CuCrO_2$ were observed in the Raman spectra, the appearance of which in the spectra are forbidden by the selection rules.[13] This confirms the phase composition of the synthesized samples. Fig. 3 shows the positions of the maxima of the main lines in the Raman spectra for different magnesium contents, which are obtained by approximating the Raman spectra using the Lorentz function.

When the magnesium content changes from $x = 0$ to $x = 0.06$, there is no systematic change in the position of the E_g lines in the Raman spectra within the error of determining the maximum. A slight tendency to shift towards increasing frequency with an increase in magnesium content up to $x = 0.03$ is observed for the A_{1g} line. The vibrational mode E_g represents triangular oscillations of the lattice perpendicular to the c axis, and the A_{1g} mode represents oscillations of O–Cu–O bonds along the c axis, *i.e.* associated with the relative displacement of layers in the delafossite structure.[13]

Consequently, the observed tendency of an increase in the frequency of oscillations of the A_{1g} mode with an increase
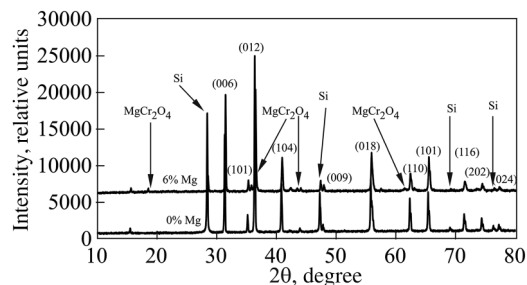

FIG. 1. X-ray diffraction patterns of synthesized copper chromite samples with the 0 and 6 at.% content of Mg.
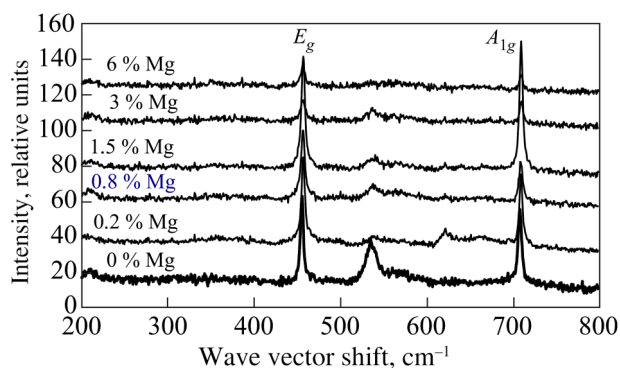
FIG. 2. Raman spectra of $CuCr_{1-x}Mg_xO_2$ samples with different magnesium content.

in the Mg content from $x = 0$ to $x = 0.03$ can be associated with a decrease in the mass of the atomic layers when Cr is replaced with lighter magnesium.

2. EFFECT OF DOPING WITH MAGNESIUM ON THE ELECTRICAL CONDUCTIVITY OF THE STUDIED SAMPLES

The temperature dependences of resistivity are studied at a wide range of temperatures below 300 K. The resistivity
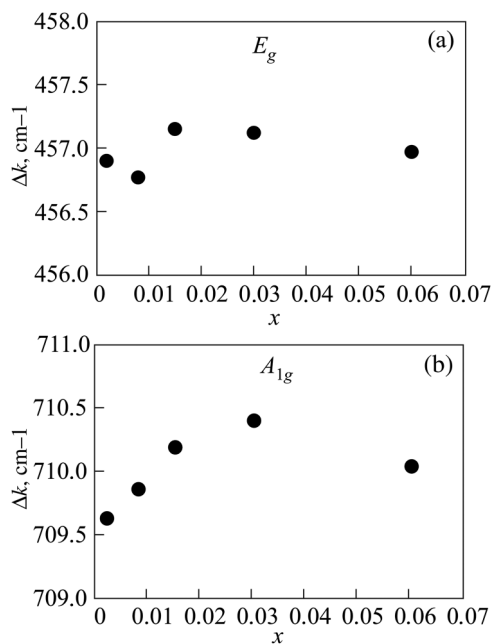

FIG. 3. The positions of the maxima of E_g (a) and A_{1g} (b) lines for different magnesium contents, which are obtained by approximating the Raman spectra using the Lorentz function.

was measured by the four-contact method with two opposite directions of current to eliminate the thermopower. The original ceramic samples are cut in the form of rectangular parallelepipeds using a diamond disc in order to measure the resistivity. The typical sizes of samples were as follows: the distance between the current contacts was 10 mm, the cross-section was 3×3 mm, the distance between the potential contacts was 3–4 mm. The contacts were made of In–Sn–Pb alloy. The measurements were carried out in a low-temperature insert in a transport Dewar vessel with liquid helium. The sample temperature was measured with a dual-junction copper/constantan thermocouple. One of the thermocouple junctions was in thermal contact with the sample, and the second was at 0°C. The temperature dependences of the resistivity ρ of the studied samples are presented in Fig. 4.

The resistivity increases rapidly with a decrease in temperature for all samples. Dependence of the resistivity on the temperature of samples with a 0 and 0.2 at.% content of Mg is described by the activation law over the entire temperature range:

$$\rho = \rho_0 \exp\left(\frac{E_a}{k_B T}\right), \tag{6}$$

where ρ is the resistivity of ceramics, ρ_0 is the pre-exponential factor, E_a is the activation energy, k_B is the Boltzmann constant, T is the temperature. This dependence is presented in Fig. 5 in $\ln \rho (1/T)$ coordinates. The activation energies for these samples are 0.28 and 0.17 eV, respectively.

At the same time, the resistivity and activation energy significantly decrease with an increase in Mg content from 0 to 6 at.%. The activation energy of electrical conductivity decreases with a decrease in temperature for samples with a magnesium content of 0.8, 1.5, 3, and 6 at.%.

In order to determine the mechanism of conductivity, let us estimate the ratio of the mean free path l of holes to the average wavelength λ for non-degenerate statistics under the assumption that the acceptor concentration is equal to the magnesium concentration, and the room
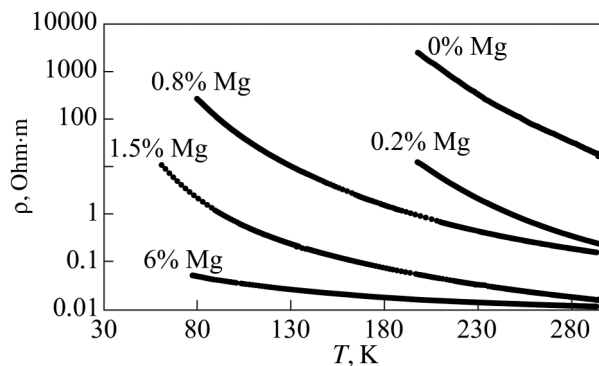

FIG. 4. Temperature dependences of the resistivity of $CuCr_{1-x}Mg_xO_2$ samples.

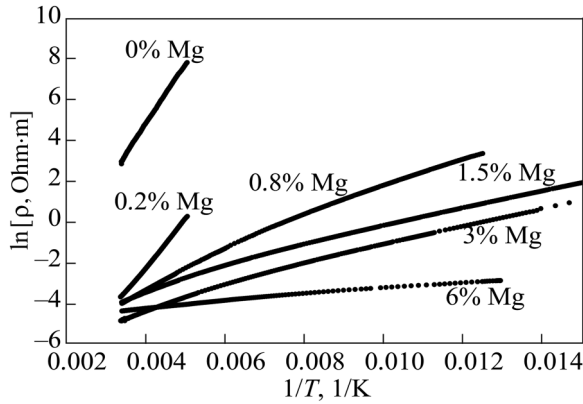**FIG. 5.** Temperature dependences of the resistivity of $CuCr_{1-x}Mg_xO_2$ samples in $\ln \rho(1/T)$ coordinates.

temperature corresponds to the impurity ionization region. In this case, the hole concentration in the valence band is determined by their activation from the impurity level, and the observed activation energy of the resistivity also determines the activation energy of the hole concentration. In these assumptions

$$\frac{1}{\lambda} = k_T l = \frac{2mk_BT}{e^2\hbar\rho\sqrt{N_{Mg}N_V}}\exp\left(\frac{E_a}{k_BT}\right), \qquad (7)$$

$$N_V = \sqrt{\frac{2}{\pi}}\frac{2\sqrt{2}(mk_BT)^{3/2}}{3\pi^2\hbar^3}, \qquad (8)$$

where N_{Mg} is the volume concentration of Mg, m is the effective mass of holes, which is assumed to be equal to the free electron mass. The results of evaluation are presented in Table 1.

The obtained $k_T l$ values are less than 1 for samples with a magnesium content of 0.8 at.% or more, which indicates the hopping mechanism of hole transfer.

In the case of hopping mechanism of conduction, a decrease in the activation energy with decreasing temperature is often associated with conductivity with a variable jump length. If the density of states near the Fermi level varies slightly in the energy range of the order of several k_BT, the resistivity

Table 1. Calculated $k_T l$ values for the $CuCr_{1-x}Mg_xO_2$ samples.

Mg content, at.%	$k_T l$
0.2	26
0.8	0.96
1.5	0.16
3	0.15
6	0.025

temperature dependence is described by Mott's law[15]:

$$\rho = \rho_0\exp\left[\left(\frac{T_0}{T}\right)^{1/4}\right], \qquad (9)$$

$$T_0 = \frac{\beta}{k_B g_F r^3}, \qquad (10)$$

where β is a numerical coefficient ($\beta = 21.2 \pm 1.2$), g_F is the density of states at the Fermi level, r is the radius of localization of the states involved in the hole transport.

A gap in the density of states can open at low temperatures near the Fermi level, which is associated with the Coulomb interaction of holes. If the gap width exceeds k_BT, the Shklovsky–Efros law[15] is satisfied for the resistivity temperature dependence:

$$\rho = \rho_0\exp\left[\left(\frac{T_1}{T}\right)^{1/2}\right], \qquad (11)$$

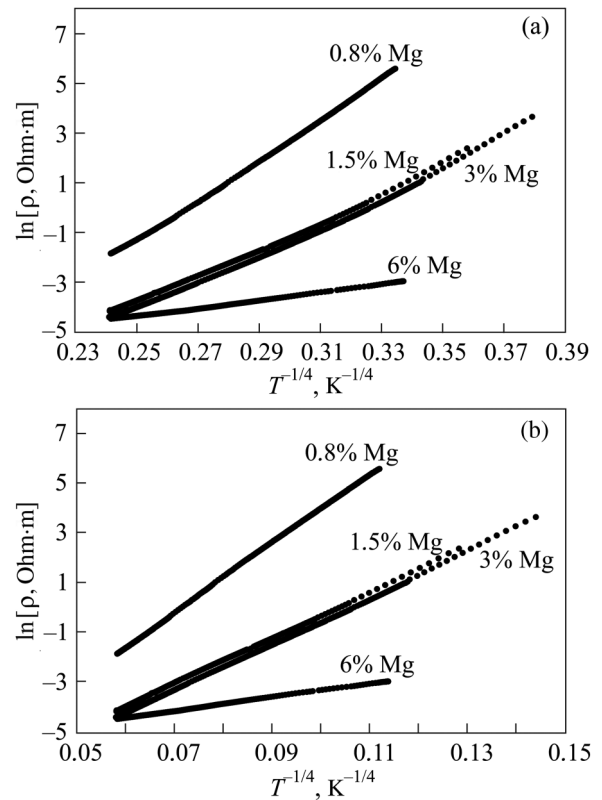$$T_1 = \frac{2.8e^2}{4\pi\varepsilon\varepsilon_0 rk_B}. \qquad (12)$$

FIG. 6. Temperature dependences of the resistivity of $CuCr_{1-x}Mg_xO_2$ samples in coordinates $\ln\rho(1/T^{1/4})$ (a) and $\ln\rho(1/T^{1/2})$ (b).

The sample resistivity temperature dependences in the coordinates $\ln\rho(1/T^{1/4})$ and $\ln\rho(1/T^{1/2})$ are shown in Fig. 6. It can be seen that the resistivity temperature dependences are better straightened in coordinates $\ln\rho(1/T^{1/2})$. This indicates the formation of a gap in the density of states near the Fermi level.

The parameters T_1, obtained as a result of approximation of the resistivity temperature dependences, are presented in Table 2. The parameter T_1 is used to estimate the radius of localization of states that contribute to the hopping conductivity. The obtained localization radius values are presented in Table 2. In order to calculate the localization radius, we used the geometric mean of the dielectric constant tensor components for the directions along and perpendicular to the c axis, which is equal to 14.[11]

3. SEEBECK COEFFICIENT OF THE STUDIED SAMPLES

Measurements of the Seebeck coefficient were carried out using the four-probe method under conditions of a constant gradient of temperature from 0.1 to 1 K. Examples of temperature dependences of the Seebeck coefficient of the studied samples are presented in Fig. 7.

A positive Seebeck coefficient was observed for all the studied samples, which corresponds to the hole conductivity. The Seebeck coefficient value decreased with a decrease in temperature. A tendency of decrease in the Seebeck coefficient with an increase in magnesium content was observed for doped samples. However, the smallest Seebeck coefficient was observed for the undoped sample.
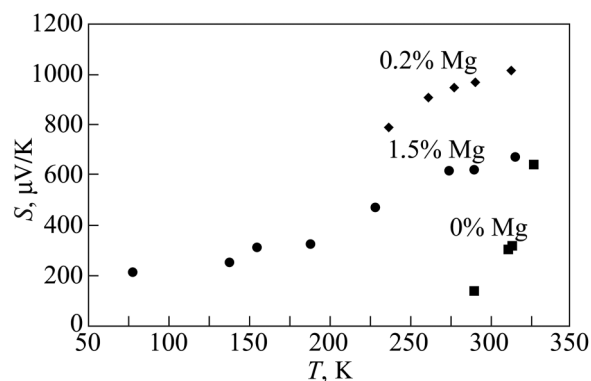
The observed values and temperature dependences of the Seebeck coefficient can be qualitatively explained within the framework of the hopping conduction mechanism established from the resistivity temperature dependences. In the case of hopping charge transport, the Seebeck coefficient is determined by the following expression[16]

$$S = \frac{1}{eT}\frac{\int (E-F)\nu(E)b(E)dE}{\int \nu(E)b(E)dE}, \qquad (13)$$

where $\nu(E)$ and $b(E)$ are the density of states and the average number of state bonds with energy E, F is the Fermi energy. This expression is positive if the product of $\nu(E)$ and $b(E)$ decreases with increasing energy. Thus, a positive sign and a high value of the Seebeck coefficient in both doped and undoped samples indicate that hole transfer occurs in localized states of the tail of the density of states of the valence

FIG. 7. Temperature dependences of the Seebeck coefficient.

band. In this case, the observed temperature dependences of the resistivity and the Seebeck coefficient can be qualitatively explained by the type of density of states and the location of the Fermi level shown in Fig. 8.

At sufficiently high temperatures for hopping charge transfer in the tails of rapidly changing density of states, the main contribution to electrical conductivity is made by jumps between states with energy close to the Fermi energy and the so-called transport energy E_t, at which the probability of a jump with an increase in hole energy has a sharp maximum.[17] As the temperature decreases, the transport level of energy shifts to the Fermi level, and the temperature dependence of the electrical conductivity changes from activation to a

Table 2. Parameters T_1 and localization radius r determined from the resistivity temperature dependences.

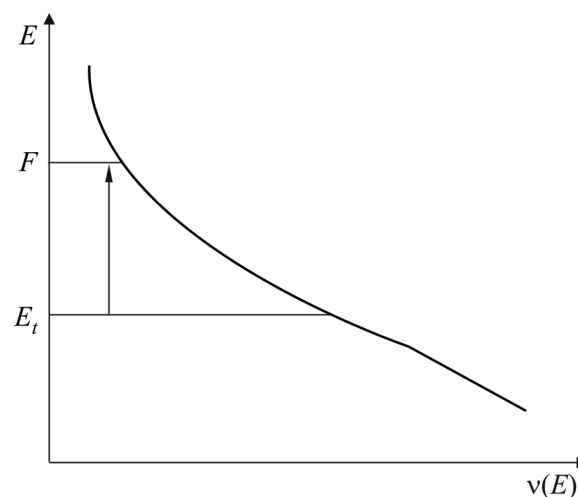| x	T_1, K	r, nm
0.008	17939	0.52
0.015	8654.74	1.08
0.03	8824.36	1.06
0.06	684.402	13.65

FIG. 8. Schematic representation of the tail of the density of states in the valence band: *F* is the Fermi energy; E_t is the transport level of energy of thermally activated jumps of holes, which make the greatest contribution to the electrical conductivity.

dependence described by the Mott's law or the Shklovsky–Efros law. The transition can be carried out in a wide range of temperatures, in which the temperature dependence of resistivity is intermediate in nature. With the existence of a transport level of energy in the activation dependence region, the activation energy is close to $F - E_t$. In this case, on the basis of the expression (8) for the Seebeck coefficient, we can obtain the following rough estimate:

$$S \approx \frac{E_A}{eT}. \qquad (14)$$

For the studied samples, the estimation according to this equation gives slightly lower values, which are, however, comparable with the experimental values of the Seebeck coefficient, for example, 195 μV/K for a sample with magnesium content $x = 0.015$ and 560 μV/K for magnesium content $x = 0.02$. The lower values compared with the experimental values obtained according to the expression (14) may be related to the fact that not only the density of states, but also the localization radius, as well as the influence of the Coulomb gap in the density of states, changes with energy.

4. ERP SPECTROSCOPY OF THE STUDIED SAMPLES

EPR spectra were measured at temperatures from 30 to 295 K in order to obtain additional information on the paramagnetic properties of the studied samples. The EPR spectra for a sample with $x = 0$ at various temperatures are presented in Fig. 9.

In the EPR spectra of both magnesium-doped and undoped samples, one broad intense line, associated with the presence of interacting chromium ions, is observed.[12] The width of this line greatly increases with a decrease in temperature, and this signal becomes almost immeasurable at a temperature below 30 K. The dependences of the EPR signal line width on temperature for samples with magnesium content of 0 and 3 at.% are shown in Fig. 10(a). Figure 10(b) shows the dependences of the relative paramagnetic susceptibility — a
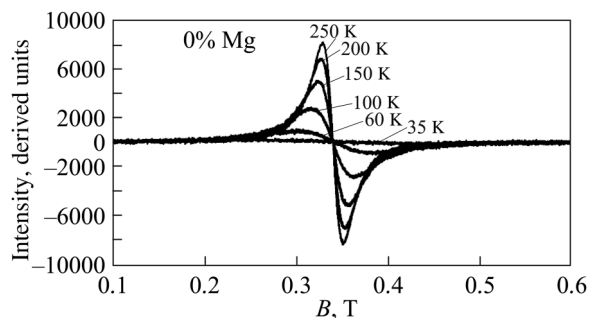
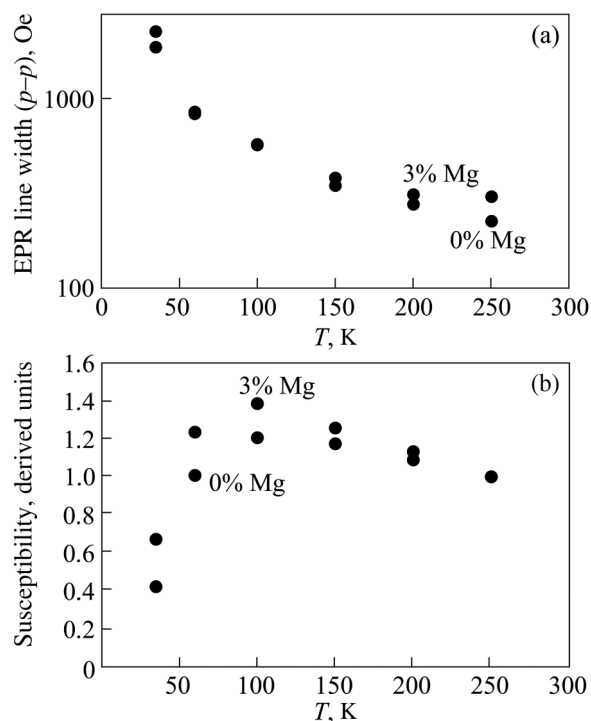**FIG. 9.** EPR spectra of a sample of copper chromite with $x = 0$ measured at various temperatures.

FIG. 10. Temperature dependences of the EPR signal line width (a) and relative paramagnetic susceptibility (b) for samples containing 0 and 3 at.% of Mg.

double-integrated EPR signal normalized to a value at 250 K for the same samples.

It can be seen that the paramagnetic susceptibility in doped samples increases with decreasing temperature from 250 to 100 K more than in the undoped sample, and the temperature dependence of the susceptibility of doped samples in the temperature range from 100–250 K is closer to the Curie–Weiss law than in the undoped sample.

This tendency is consistent with the results of direct measurements of the magnetic susceptibility of magnesium doped copper chromite[18] and can be explained by the partial replacement of magnetic chromium ions by nonmagnetic magnesium ions in a quasi-two-dimensional frustrated lattice. An increase in the EPR line width upon doping with magnesium can be associated with an increase in the electrical conductivity and, accordingly, the absorption of electromagnetic radiation in the samples.

CONCLUSION

Ceramic samples of copper chromite with a magnesium content of 0, 0.2, 0.8, 1.5, 3, and 6 at.% were synthesized using a method that ensures a uniform distribution of the dopant. X-ray diffraction analysis showed that samples with magnesium content of up to 3 at.% are single-phased. The phase composition of the samples was confirmed by Raman spectroscopy. The A_{1g} line shift with an increase in magnesium content indicated

that chromium is replaced by magnesium in the crystal lattice, which was confirmed by a change in the temperature dependences of the EPR spectra upon doping with magnesium.

The temperature dependences of resistivity and the Seebeck coefficient of the synthesized samples were measured over a wide range of temperatures. The hole conduction type is confirmed by a positive sign of the Seebeck coefficient. Verification of the Joffe–Regel criterion demonstrated that the hopping mechanism of hole transport prevails in magnesium-doped samples.

According to the analysis of the resistivity temperature dependences, we obtained estimates of the localization radius of the states involved in hole transport. It is shown that the temperature dependences of the resistivity and the Seebeck coefficient for doped samples can be explained by the hole transfer in the tail of the density of states near the valence band.

REFERENCES

[1] R. Daoua, R. Frésarda, V. Eyerta, S. Héberta, and A. Maignana, Sci. Technol. Adv. Mater. **18**, 919 (2017).

[2] J. Tate, H. L. Ju, J. C. Moon, A. Zakutayev, A. P. Richard, J. Russell, and D. H. McIntyre, Phys. Rev. B **80** 165206 (2009).

[3] M. J. Han, Z. H. Duan, J. Z. Zhang S. Zhang, Y. W. Li Z. G. Hu, J. H. Chu, J. Appl. Phys. **114**, 163526 (2013).

[4] Y. Ono, K. Sato, T. Nozaki, and T. Kajitani, Jpn. J. Appl. Phys. **46**, 1071 (2007).

[5] Y. Wang, Y. Gu, and T. Wang, J. Alloys and Compounds **509**, 5897 (2011).

[6] D. Li, X. Fang, Z. Deng, S. Zhou, R. Tao, W. Dong, T. Wang, Y. Zhao, G. Meng, and X Zhu, J. Phys. D Appl. Phys. **40**, 4910 (2007).

[7] T. S. Tripathi and M. Karppinen, Adv. Electr. Mater. **3**, 1600341 (2017).

[8] I. Sinnarasa, Y. Thimont, L. Presmanes, A. Barnabé, and P. Tailhades, Nanomater. **7**, 157 (2017).

[9] R. Gillen and J. Robertson, Phys. Rev. B **84**, 035125 (2011).

[10] D. O. Scanlon and G. W. Watson, J. Mater. Chem. **21**, 3655 (2011).

[11] M. Poienar, V. Hardy, B. Kundys, K. Singh, A. Maignan, F. Damay, and C. Martin, J. Solid State Chem. **185**, 56 (2012).

[12] M. Hemmida, H.-A.K. von Nidda, N. Büttgen, A. Loidl, L. K. Alexander, R. Nath, and A. V. Mahajan, Phys. Rev. B **80**, 054406 (2009).

[13] A. B. Garg, A. K. Mishra, K. K. Pandey, and S. M. Sharma, J. Appl. Phys. **116**, 133514 (2014).

[14] A. M. Vasiliev, L. A. Prozorova, L. E. Svistov, V. Tsurkan, V. Dziom, A. Shuvaev, Anna Pimenov, and A. Pimenov, Phys. Rev. B **88**, 144403 (2013).

[15] B. I. Shklovsky and A. L. Efros, *Electronic Properties of Doped Semiconductors*, Moscow (1979).

[16] I. P. Zvyagin, *Kinetic phenomena in disordered semiconductors*, Moscow (1984).

[17] D. Monroe, Phys. Rev. Lett. **54**, 146 (1985).

[18] T. Okuda, N. Jufuku, S. Hidaka, and N. Terada, Phys. Rev. B **72**, 144403 (2005).

Translated by AIP Author Services